AGU PUBLICATIONS

Geophysical Research Letters

RESEARCH LETTER
10.1002/2017GL073042

Key Points:
- The structure of the Canada Basin halocline is examined in context with its seasonal ventilation by Chukchi Sea waters
- We show how surface Chukchi Sea water is transferred by subduction into the halocline
- We demonstrate how the warm halocline is preserved year round because it is isolated by stratification (vertically and laterally) in winter

Supporting Information:
- Supporting Information S1

Correspondence to:
M.-L. Timmermans,
mary-louise.timmermans@yale.edu

Citation:
Timmermans, M.-L., J. Marshall, A. Proshutinsky, and J. Scott (2017), Seasonally derived components of the Canada Basin halocline, *Geophys. Res. Lett.*, *44*, 5008–5015, doi:10.1002/2017GL073042.

Received 13 FEB 2017
Accepted 19 APR 2017
Accepted article online 24 APR 2017
Published online 26 MAY 2017

Seasonally derived components of the Canada Basin halocline

Mary-Louise Timmermans[1], John Marshall[2], Andrey Proshutinsky[3], and Jeffery Scott[2]

[1]Department of Geology and Geophysics, Yale University, New Haven, Connecticut, USA, [2]Department of Earth, Atmospheric and Planetary Sciences, Massachusetts Institute of Technology, Cambridge, Massachusetts, USA, [3]Woods Hole Oceanographic Institution, Woods Hole, Massachusetts, USA

Abstract The Arctic halocline stratification is an important barrier to the transport of deep ocean heat to the underside of sea ice. Surface water in the Chukchi Sea, warmed in summer by solar radiation, ventilates the Canada Basin halocline to create a warm layer below the mixed-layer base. The year-round persistence of this layer is shown to be consistent with the seasonal cycle of halocline ventilation. We present hydrographic observations and model results to show how Chukchi Sea density outcrops migrate seasonally as surface fluxes modify salinity and temperature. This migration is such that in winter, isopycnals bounding the warm halocline are blocked from ventilation, while the cool, relatively salty and deeper halocline layers are ventilated. In this way, the warm halocline is isolated by stratification (both vertically and laterally) each winter. Results shed light on the fate and impact to sea ice of the warm halocline under future freshening and warming of the surface Arctic Ocean.

1. Introduction

The Arctic Ocean's Canada Basin has a strong halocline stratification, with upper layers formed and modified by inflows from the Pacific Ocean, sea ice melt/growth, net precipitation, river runoff, and redistribution of surface freshwater by atmospheric forcing [e.g., *Aagaard et al.*, 1981]. The anticyclonic Beaufort Gyre dominates the large-scale ice and ocean circulation in the Canada Basin [e.g., *Proshutinsky et al.*, 2009]. In general, the Canada Basin halocline consists of a lower portion of relatively cold and salty waters (the cold halocline) underlying an upper portion composed of relatively fresh and typically warmer waters (the warm halocline), Figure 1.

The canonical picture of formation and maintenance of the cold halocline is that dense water created by freezing and brine rejection over the shelf regions of the Arctic sinks to its level of neutral buoyancy and spreads laterally into the interior basin [e.g., *Aagaard et al.*, 1981; *Melling and Lewis*, 1982; *Melling*, 1993; *Aagaard and Carmack*, 1994; *Weingartner et al.*, 1998; *Wells and Wettlaufer*, 2007]. The mechanism for lateral spreading to the interior remains unclear, although it is believed to be aided by eddy fluxes and wind-driven upwelling/downwelling and associated lateral exchange [e.g., *Spall et al.*, 2008; *Woodgate et al.*, 2005a; *Williams and Carmack*, 2015; *Jackson et al.*, 2015]. The warm halocline layers are thought to originate from warm surface waters at the basin margins in summer [e.g., *Steele et al.*, 2004; *Morison et al.*, 2012; *Timmermans et al.*, 2014; *Brugler et al.*, 2014]. *Timmermans et al.* [2014] put forward that the Canada Basin warm halocline is ventilated by a combination of wind-driven Ekman pumping and the large-scale geostrophic circulation; in summer, water is transferred from the surface in the Chukchi Sea into the halocline by wind-driven Ekman convergence and subduction (i.e., lateral induction plus Ekman pumping) in regions where warm water masses with the same properties as those in the Canada Basin halocline outcrop at the surface, analogous to thermocline ventilation in the midlatitudes [e.g., *Iselin*, 1939; *Stommel*, 1979; *Luyten et al.*, 1983]. The key element here is that there is a clear physical mechanism for penetration of waters into the interior: they are swept along geostrophic contours downward and northward into the gyre, following a helical pathway [*Timmermans et al.*, 2014].

Here we focus on understanding halocline ventilation by water that leaves the surface in the Chukchi Sea (Chukchi Shelf Water, CSW), within which we include the Canada Basin boundary region off the coast of Alaska. CSW is derived primarily from water flowing north through Bering Strait year round, with a smaller fraction in the form of influxes from the Siberian Coastal Current [e.g., *Weingartner et al.*, 1998; *Woodgate et al.*, 2005b, 2015]. Superimposed on the seasonal cycle of waters entering through Bering Strait [*Woodgate et al.*, 2005b], waters over the Chukchi Shelf are freshened by ice melt and summer river influxes, and warmed

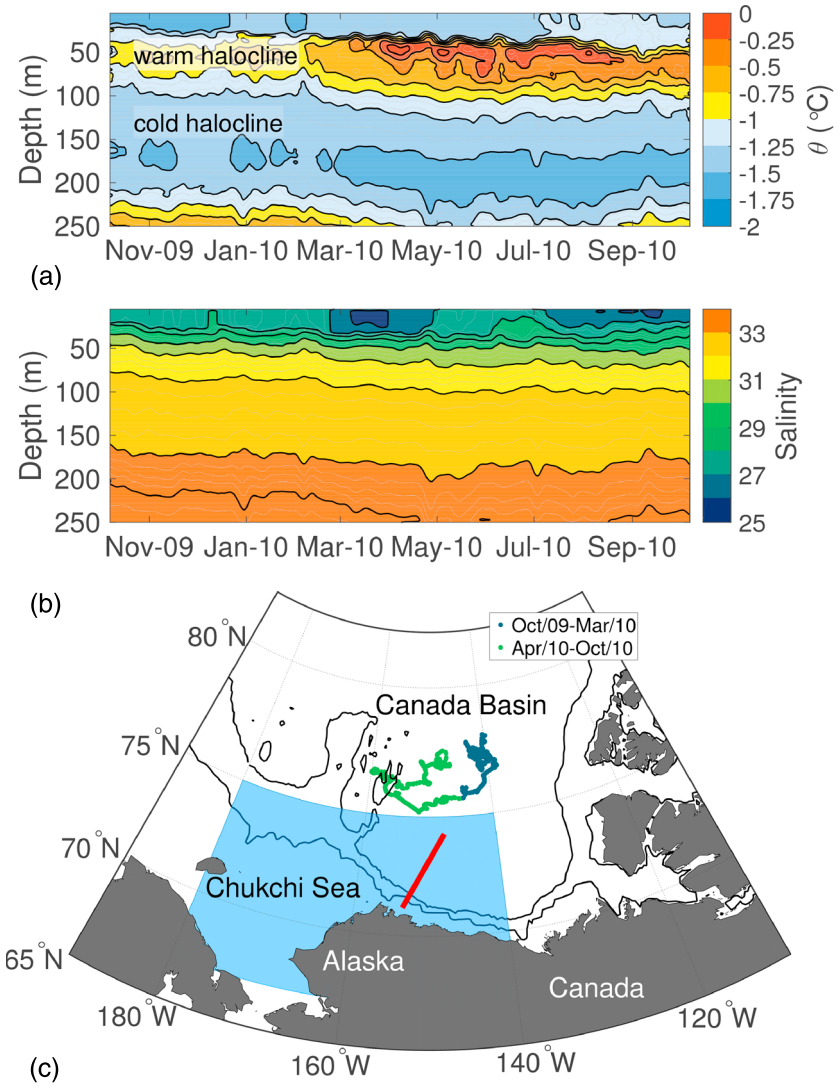

Figure 1. Time-depth sections of (a) potential temperature (θ, °C, referenced to zero pressure) and (b) salinity S from (c) the yearlong drift track (profile locations colored by date as shown in the legend) of an Ice-Tethered Profiler (ITP 33) that sampled in the Canada Basin between October 2009 and October 2010. While the temporal section aliases spatial variability over the ITP drift region, introducing a measure of perceived temporal variability (water column fluctuations), the general features are robust (i.e., there are no major water mass fronts in the sampling region). Bathymetric contours in Figure 1c are 1000 m and 100 m, and the red line marks the location of the vertical section shown in Figure S4. The blue shaded region indicates the area over which we compute subduction (Figure 3).

by insolation in summer (to form summer CSW: sCSW), and are cooled and then made more saline by ice growth and mechanical mixing in winter (to form winter CSW: wCSW). CSW may take values within the approximate salinity range $25 < S < 34$, with significant seasonal and interannual variations that depend upon the source water properties, ice cover, and atmospheric conditions.

In this study, we consider the temperature and salinity (T-S) structure of the halocline in the Canada Basin as it relates to its source sCSW and wCSW. Most importantly, we explain the thermodynamics and dynamics that allow for the year-round persistence of the warm halocline (centered around 50 m depth) below the mixed layer in the Canada Basin (Figures 1a and 1b). In section 2, we review the structure of the Canada Basin halocline as it relates to Chukchi Sea water masses that are transformed over an annual cycle. Oceanographic measurements, particularly in the important Chukchi shelf/slope regions and in winter, are insufficient to test ventilation hypotheses. Therefore, we employ an Arctic model based on the Massachusetts Institute of Technology (MIT) general circulation model, MITgcm [*Marshall et al.*, 1997a, 1997b; *Adcroft et al.*, 2004] to explore the dynamical connection between CSW and the structure of the Canada Basin halocline through

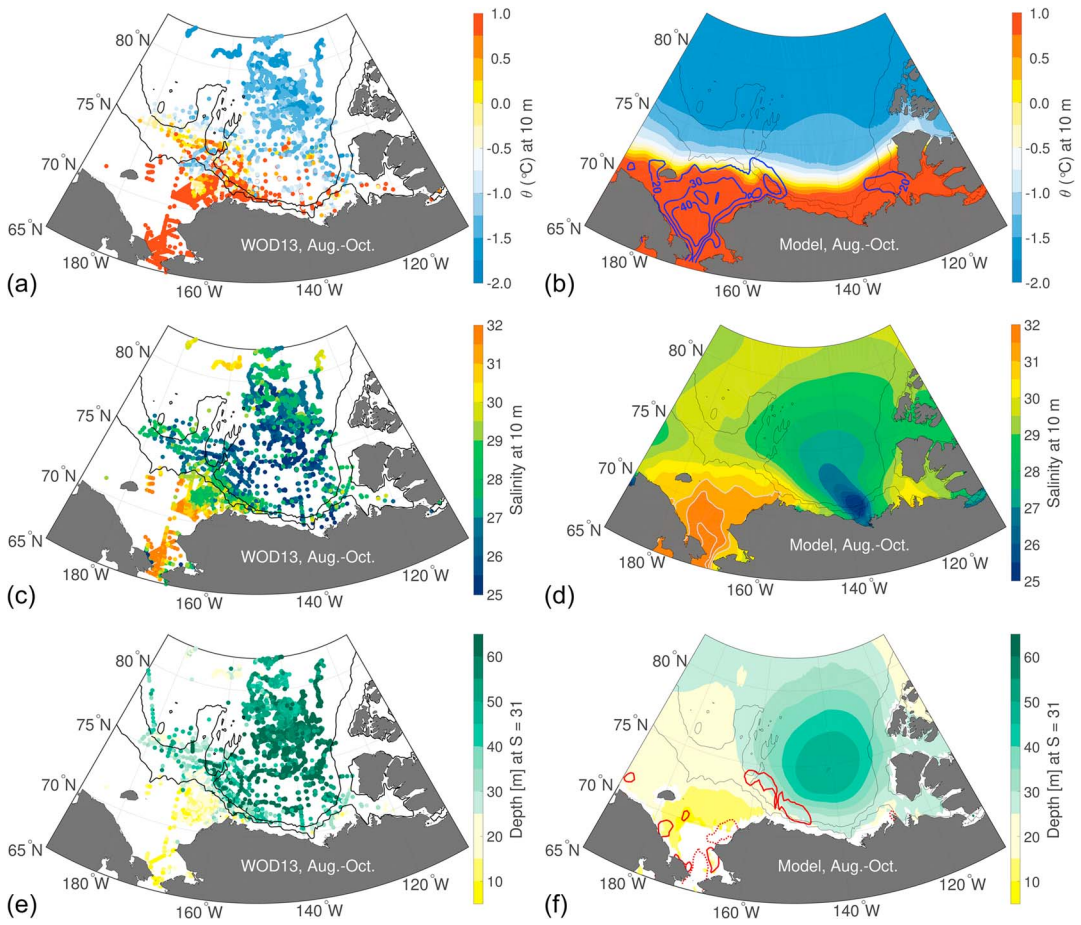

Figure 2. Maps of (a, b) potential temperature (°C) and (c, d) salinity at 10 m depth (grey contours in Figure 2d indicate $S = 31$, 31.5, and 32) and (e, f) depth (m) of the $S = 31$ isohaline between 2003 and 2013 for the months of August–October. The maps in Figures 2a, 2c, and 2e are derived from hydrography archived at the 2013 World Ocean Database (WOD13; http://www.nodc.noaa.gov/OC5/WOD13/), and Figures 2b, 2d, and 2f are model output. Bathymetric contours (black) are 1000 m and 100 m. Blue contours in Figure 2b indicate model mixed-layer depth (m), using a density difference from the shallowest measurement criterion of 0.05 kg/m^3, for October 2009; see the full field in Figure S2a. Red contours in Figure 2f indicate model subduction (40 cm/d, solid; −40 cm/d, dashed) at the base of the mixed layer (positive down) in October 2009 (see the full field in Figure S2c); maximum/minimum subduction regions are within these contours, with much weaker magnitude subduction ($|Su| \lesssim 10$–20 cm/d) over the rest of the domain.

analysis of model monthly mean fields of T, S, and velocity. The basic mechanism proposed for seasonal variability in halocline ventilation is described in section 3 where we analyze the magnitude and seasonal cycle of halocline ventilation by Chukchi Shelf waters. Our results are summarized and discussed in section 4.

2. Oceanographic Setting

We begin by noting that the general upper ocean structure and water mass distribution in the model output are in broad agreement with hydrographic observations (Figure 2). Briefly, the coupled ocean and sea ice model [see *Heimbach et al.*, 2010] is forced by reanalysis [*Onogi et al.*, 2007] for the period 1979–2013; initial and open-boundary conditions are specified from hydrographic climatology and optimized simulations [*Gouretski and Koltermann*, 2004; *Nguyen et al.*, 2011]. The ocean model has a mean horizontal grid spacing ~36 km and consists of 50 vertical levels (~5–10 m vertical resolution near the surface). Model runs have eddy diffusivity set to $K = 50$ m^2 s^{-1} in the Gent-McWilliams (GM) parameterization.

The upper ocean structure in the Chukchi Sea/Canada Basin region is characterized by a relatively fresh Beaufort Gyre centered over the Canada Basin, with saltier surface waters to the southwest in the Chukchi Sea (Figure 2). The dominant feature is a surface front in the vicinity of the Chukchi slope; the strongest lateral

gradient in surface salinity is roughly aligned with the 100 m isobath (Figures 2c and 2d). The frontal region is also characterized by the strongest lateral gradients in mixed-layer depth, with deeper mixed layers to the south (Figure 2b). The front is maintained by inflowing Pacific water and strengthened by the large-scale anticyclonic atmospheric forcing. This atmospheric forcing drives the main Beaufort Gyre circulation, evident in the distribution of the depth of the $S = 31$ isohaline (an isohaline characterizing the warm halocline of the Canada Basin), which is deepest in the central Canada Basin/Beaufort Gyre region and shoals in the boundary regions, including the Chukchi Sea (Figures 2e and 2f). Although there is some seasonal variability, this general large-scale pattern holds throughout the year (compare August–October, Figure 2, to January–March, Figure S1 in the supporting information). The exception to this falls at the onset of the melt season, and into midsummer, when shallow mixed layers and a broad distribution of freshwater generally characterize the entire region (i.e., the lateral gradient in mixed-layer depth is significantly reduced). As an aside, the local surface salinity minimum offshore of the Mackenzie River outflow (Figure 2d, around 138°W) appears to be a circulation feature associated with the particular confluence of topography, freshwater input to the surface, and wind forcing [see, e.g., *Williams and Carmack*, 2015, Figures 5 and 10; *Fichot et al.*, 2013].

In the Canada Basin interior, the halocline is characterized by a marked warm temperature layer (with maximum temperatures around 0°C at around 50 m depth, although with significant spatial and interannual variability in these values) within the salinity range of about $30 < S < 32$ and cooler temperatures (~−1.5°C, centered around 150 m depth) within the approximate salinity range $32 < S < 33$ (Figures 1a and 1b). The past decade has seen general warming (and increased heat content) of warm halocline water in the Canada Basin, with considerable interannual variability (with the maximum temperature varying by up to 1°C between years), although with no apparent seasonal variability in the warm halocline [*Timmermans et al.*, 2014]. Observations are consistent with changes in sCSW; for example, anomalously warm temperatures in the warm halocline in 2007 are associated with warm anomalies in the Chukchi Sea that same year [*Timmermans et al.*, 2014].

Seasonal changes in CSW are manifest in the structure of the Canada Basin halocline. Outcropping isohalines at a given latitude in the Chukchi Sea are warmer and fresher in summer ($S \approx 30–32$) than they are in winter ($S \gtrsim 32$); see Figures 2 and S1. Next we show how the seasonal migration of density outcrops affects halocline ventilation.

3. Halocline Ventilation

The fundamental mechanism for halocline ventilation of relevance here is that water on isopycnals outcropping in the Chukchi Sea is transported into the interior Canada Basin halocline by Ekman pumping and lateral induction. Subducting water masses move down and laterally along isopycnals as they are conveyed along Beaufort Gyre geostrophic contours. Subduction Su (i.e., the vertical velocity of a parcel of water with respect to the base of the mixed layer, on an f plane) is the sum of vertical Ekman velocity w_E (negative downward) and lateral induction $\mathbf{u_h} \cdot \nabla h$, where $\mathbf{u_h} = (u_h, v_h)$ is the horizontal velocity at the base of the mixed layer of depth $h(x, y)$ [e.g., *Nurser and Marshall*, 1991]:

$$Su = -w_E + \mathbf{u_h} \cdot \nabla h. \tag{1}$$

$Su > 0$ for water leaving the mixed layer.

Su is computed from monthly model output using w_E and $\mathbf{u_h}$ at the base of the mixed layer, where mixed-layer depth h is estimated using a 0.05 kg m^{-3} density difference from the shallowest measurement criterion (visual inspection for a range of conditions suggests that this returns reliable estimates; the mixed-layer depth returned is not sensitive to the exact density difference criterion). The Ekman velocity is the vertical velocity output of the coupled ocean and sea ice model (i.e., accounting for wind stress and the presence of sea ice) [see, e.g., *Bigdeli et al.*, 2017]. Near the basin margins, Ekman velocities (taking values up to 50–100 cm/d) can account for most of the total subduction. The same is true in the interior Canada Basin where mixed-layer depths do not vary significantly, and weak subduction mainly results from Ekman pumping. However, lateral induction dominates subduction in the frontal region, approximately along the 100 m isobath separating the Chukchi Sea and Canada Basin, where lateral gradients in salinity and mixed-layer depth are strongest. This is the region of strongest positive Su (Figures 2f, S1f, S2c, and S2d); here in both October and March (representative of summer/fall and winter/spring, respectively), monthly mean Su attains values of more than 50 cm/d.

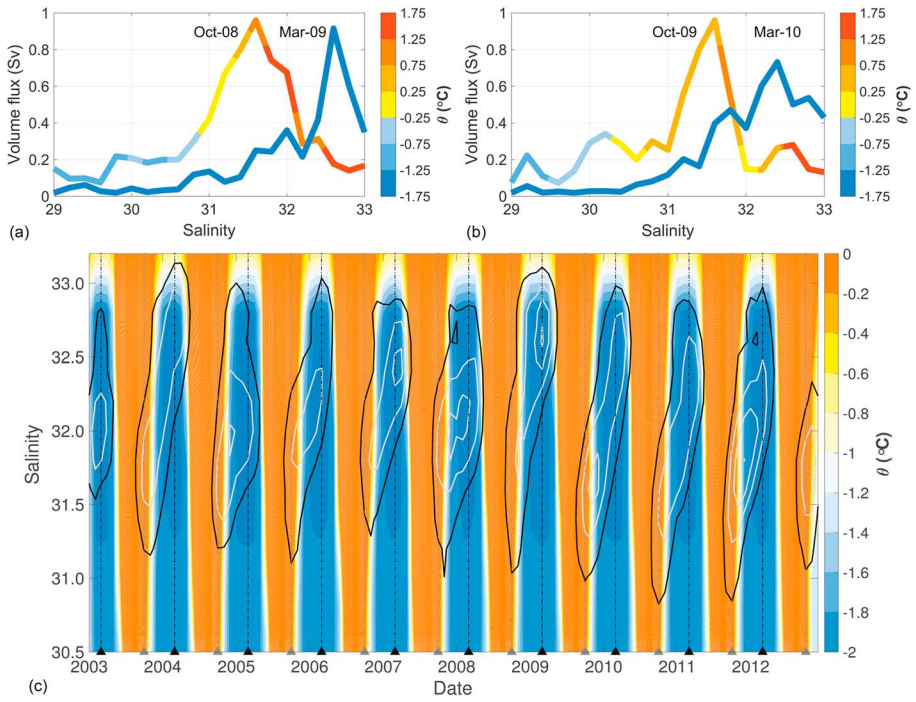

Figure 3. Volume flux (Sv, where 1 Sv = 10^6 m^3 s^{-1}) ventilating the halocline versus salinity for (a) October 2008 and the following March 2009, and (b) October 2009 and March 2010. The volume flux is positive subduction (i.e., water of a given salinity, for a bin size of 0.2, leaving the mixed layer), computed as the sum of vertical velocity and lateral induction at the base of the mixed layer, multiplied by the area of a given grid cell; colors indicate the mean potential temperature (°C) of water leaving the mixed layer. The calculation was performed on the monthly model output over a region spanning 67°N to 75°N and 180–140°W (see Figure 1c). (c) Potential temperature (°C, color) and volume flux (Sv, contours) into the halocline of water of a given salinity versus time. Potential temperatures warmer than 0°C are colored by the warmest color on the scale. The volume flux contours are 0.3 Sv (black) surrounding, each year, white contours in increments of +0.2 Sv. Black and grey notches on the *x* axis indicate (for each year) March and October, respectively.

To understand halocline ventilation by CSW, we estimate net positive subduction (i.e., water leaving the surface) over a region bounded by 67–75°N and 180–140°W (Figure 1c). The exact choice of domain makes little difference to the results because the main subduction region is concentrated close to the southwest boundaries of the Canada Basin and along the 100 m isobath in the Chukchi Sea (Figure 2f). Model grid cells characterized by positive *Su* have water parcels leaving the mixed layer in a given month. A positive value of *Su* characterizing a given grid cell is multiplied by the cell area to estimate a volume flux of water leaving the mixed layer in that cell. To capture wintertime ventilation of the cold halocline (sourced from wCSW), and summertime ventilation of the warm halocline (sourced from sCSW), we consider only those grid cells with mixed-layer water of salinity within the range of salinity values relevant to those water masses. The specified mixed-layer salinity range is taken to be $S = 30–33$ (with a bin size of 0.2), to encompass both the warm halocline and cold halocline (see Figure 1). The result is a net subduction of halocline water within the domain as a function of salinity within the chosen range (Figure 3). The net subduction in October is predominantly water characterized by a salinity of 31 to 32 and temperatures above freezing (sCSW), while the March subduction is of cooler water having a salinity between 32 and 33 and temperatures around freezing, wCSW (Figures 3a and 3b). This seasonal pattern is repeated each year (Figure 3c). There is minimal subduction in June, July, and August when thin, fresh mixed layers dominate the entire region after the onset of the melt season. Beginning in September/October, subduction increases, and there are no consistent differences between summer/fall and winter/spring ventilation rates in model output spanning 2003–2013 (Figure 3c).

For the salinity ranges noted above (i.e., $31 < S < 32$ bounding the peaks in Figures 3a and 3b), mean subduction in the region is about 0.4–0.6 Sverdrup (Sv) (1 Sv = 10^6 m^3 s^{-1}). This is a rate of about 10^{12} m^3 $month^{-1}$, which suggests that over a couple of months, about one fifth of the warm halocline in the Canada Basin can

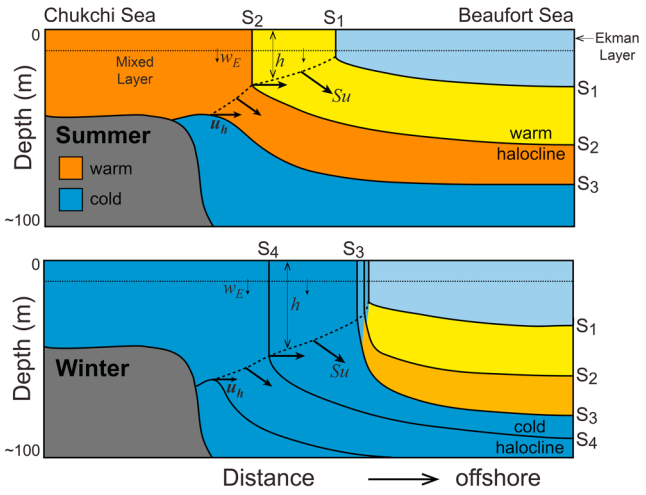

Figure 4. Schematic depth-distance section from the Chukchi Sea/Canada Basin boundaries to the interior Canada Basin showing isohalines in (top) summer and (bottom) winter. Isohalines may be taken to be approximately $S_1 \approx 30$ to $S_4 \approx 33$, although with variations in these values as forcing and sources vary in any given year and season. This illustrates how the warm halocline survives through the winter (i.e., the warm layer is not displaced by near-freezing water ventilating in winter).

be ventilated (taking the area to be about 2×10^5 km^2 and the thickness of the warm halocline to be about 50 m). That is, it is likely that *T* and *S* properties of outcropping sCSW in any given summer will be observed in the properties of the warm Canada Basin halocline that same year. To test these estimates, we released a passive tracer at the ocean surface in both October 2009 and March 2010 over the region of strongest subduction (Figure S3). Water parcels are observed to sweep around the Beaufort Gyre anticyclonically, following a broad trajectory to the center [see *Timmermans et al.*, 2014]. There is also some mixing across geostrophic contours with eddies transported by a bolus velocity in the GM parameterization. Tracers indicate that water from the Chukchi Sea penetrates the interior gyre, with pathways entering from the southwest and west, in about 6 months to 2 years (whether the tracer is released in October or March, Figure S3). It is worth noting that the estimated subduction rate of CSW leaving the surface (around 0.4 Sv) is a substantial fraction of the total volume transport through Bering Strait (estimated to be about 1 Sv) [*Woodgate et al.*, 2015].

Seasonal water mass variation of CSW leads to less dense, shallower (fresher and warmer) waters being ventilated in the Canada Basin halocline in summer and more dense, deeper (saltier and colder) waters being ventilated in winter (Figure 3); this is depicted schematically in Figure 4. Northward migration in winter of CSW outcropping isopycnals bounding the summer halocline leads to a configuration that does not allow for ventilation of water masses of that salinity class in winter. *Timmermans et al.* [2014] show examples where lateral gradients in surface temperature-salinity values from the Chukchi Sea to the Canada Basin approximately map on to vertical profiles, from shallow to deep, in the Canada Basin. This provides evidence for the movement of water from the Chukchi Sea surface down and laterally into the Canada Basin halocline. A similar mapping structure, albeit with some modification by mixing of subducted waters, can be seen in October (representative of late summer/fall conditions) and March (representative of winter/spring conditions) model temperature and salinity sections from the shelf regions to the Canada Basin interior (Figure S4).

4. Summary and Discussion

Seasonal variability of CSW properties is key to the presence of the warm layer found year round in the Canada Basin halocline. Seasonal north/south migration of density (salinity) outcrops in the Chukchi Sea/Canada Basin is such that the warm halocline is ventilated in summer, while the cold Canada Basin halocline is ventilated each winter (compare to seasonal surface density changes in the Atlantic Ocean that are manifest in thermocline structure [*Marshall et al.*, 1999]). Ventilation timescales estimated here suggest that about one fifth of the warm halocline in the central Canada Basin could be renewed by subduction of warm sCSW in one summer/fall (i.e., changes in the Canada Basin halocline could reflect characteristics of CSW at the surface in the Chukchi Sea that same year).

Summer sea surface temperatures in the Chukchi Sea have been warming at a rate of about 0.5°C per decade since 1982 [*Timmermans and Proshutinsky*, 2016], and this warming has already been seen in the warm halocline of the Canada Basin [*Timmermans et al.*, 2014]. With continued warming of sCSW, additional heat will continue to be archived in the warm halocline. However, the framework described here sets important limitations on halocline ventilation and archival of warm waters there. With continued warming sCSW may become sufficiently warm that its density is modified such that the lateral density gradient in the vicinity of

the Chukchi slope is diminished; although the waters are presently warming, their temperatures are still sufficiently cool that the coefficient of thermal expansion is small, and warming has negligible effect on density [see *Timmermans and Jayne*, 2016]. Elimination of the surface front discussed here shuts off a major conduit for halocline ventilation. Similarly, continued freshening at the Canada Basin margins and Chukchi Sea will also put an end to summer halocline ventilation.

Presently, the low salinity of the central Canada Basin/Beaufort Gyre, plus weak buoyancy fluxes and mechanical mixing, limit winter mixed-layer depths and largely prevent reentrainment of the summer halocline. This is an important distinction from dynamics of thermocline ventilation where only winter mixed-layer water can be permanently subducted [*Stommel*, 1979]. In the case of thermocline ventilation, *Stommel* [1979] argued that only water leaving the wintertime mixed layer enters the permanent thermocline because vertical mixing in the winter ultimately reentrains waters that have left the mixed layer in spring, summer, and fall. While the Canada Basin surface ocean is not presently subject to sufficiently strong vertical mixing in winter to erode the warm halocline [see, e.g., *Timmermans*, 2015], entrainment of this heat would have serious consequences to sea ice cover. Integrated heat content with respect to the freezing temperature of the warm halocline layer (Figure 1a; the integration is taken between isohalines $S = 29$ and $S = 32$) is about 3×10^8 J m^{-2}. If all of this heat were to be entrained to the surface, this would amount to about 1 m of sea ice melt, taking the latent heat of melting to be 2.67×10^5 J kg^{-1} and the density of sea ice to be 900 kg m^{-3}.

Finally, results here point to several key ocean properties that ultimately set the structure of the interior Canada Basin halocline: spatial patterns and temporal evolution of surface temperature, salinity, mixed-layer depth, and velocity in the Chukchi Sea and southwest Canada Basin. Sustained ocean observations are needed in this region to understand how the interplay between surface water masses at the margins and variable wind forcing and sea ice cover controls the interior halocline.

Acknowledgments
The MITgcm is an open-source code available online at http://mitgcm.org/. The Ice-Tethered Profiler data were collected and made available by the Ice-Tethered Profiler Program based at the Woods Hole Oceanographic Institution [*Krishfield et al.*, 2008; *Toole et al.*, 2011]. Hydrographic data are from the World Ocean Database 2013 (WOD13), available at https://www.nodc.noaa.gov/OC5/WOD/pr_wod.html. Partial support was provided by the National Science Foundation Division of Polar Programs under awards 1350046 and 1603542.

References

Aagaard, K., and E. Carmack (1994), The Arctic Ocean and climate: A perspective, in *The Polar Oceans and Their Role in Shaping the Global Environment, Geophys. Monogr. Ser.*, vol. 85, edited by O. M. Johannessen, R. D. Muench, and J. E. Overland, pp. 5–20, AGU, Washington, D. C.

Aagaard, K., L. Coachman, and E. Carmack (1981), On the halocline of the Arctic Ocean, *Deep Sea Res. Part A*, *28*(6), 529–545.

Adcroft, A., J. Campin, C. Hill, and J. Marshall (2004), Implementation of an atmosphere-ocean general circulation model on the expanded spherical cube, *Mon. Weather Rev.*, *132*, 2845–2863, doi:10.1175/MWR2823.1.

Bigdeli, A., B. Loose, A. T. Nguyen, and S. T. Cole (2017), Numerical investigation of the Arctic ice-ocean boundary layer and implications for air-sea gas fluxes, *Ocean Sci.*, *13*, 61–75, doi:10.5194/os-13-61-2017.

Brugler, E. T., R. S. Pickart, G. Moore, S. Roberts, T. J. Weingartner, and H. Statscewich (2014), Seasonal to interannual variability of the Pacific water boundary current in the Beaufort Sea, *Prog. Oceanogr.*, *127*, 1–20.

Fichot, C. G., K. Kaiser, S. B. Hooker, R. M. W. Amon, M. Babin, S. Bélanger, S. A. Walker, and R. Benner (2013), Pan-Arctic distributions of continental runoff in the Arctic Ocean, *Sci. Rep. Nat. Publ. Group*, *3*, 1053.

Gouretski, V., and K. Koltermann (2004), WOCE Global Hydrographic Climatology, *Tech. Rep.*, 52 pp., Berichte des Bundesamtes 20 fur Seeschifffahrt und Hydrographie.

Heimbach, P., D. Menemenlis, M. Losch, J.-M. Campin, and C. Hill (2010), On the formulation of sea-ice models. Part 2: Lessons from multi-year adjoint sea-ice export sensitivities through the Canadian Arctic Archipelago, *Ocean Modell.*, *33*(1), 145–158.

Iselin, C. (1939), The influence of vertical and lateral turbulence on the characteristics of the waters at mid-depths, *Eos Trans. AGU*, *20*, 414–417.

Jackson, J. M., H. Melling, J. V. Lukovich, D. Fissel, and D. G. Barber (2015), Formation of winter water on the Canadian Beaufort shelf: New insight from observations during 2009–2011, *J. Geophys. Res. Oceans*, *120*, 4090–4107, doi:10.1002/2015JC010812.

Krishfield, R., J. Toole, A. Proshutinsky, and M.-L. Timmermans (2008), Automated Ice-Tethered Profilers for seawater observations under pack ice in all seasons, *J. Atmos. Oceanic Technol.*, *25*, 2091–2095.

Luyten, J., J. Pedlosky, and H. Stommel (1983), The ventilated thermocline, *J. Phys. Oceanogr.*, *13*, 292–309.

Marshall, J., A. Adcroft, C. Hill, L. Perelman, and C. Heisey (1997a), A finite-volume, incompressible Navier-Stokes model for studies of the ocean on parallel computers, *J. Geophys. Res.*, *102*, 5753–5766.

Marshall, J., C. Hill, L. Perelman, and A. Adcroft (1997b), Hydrostatic, quasi-hydrostatic, and nonhydrostatic ocean modeling, *J. Geophys. Res.*, *102*(C3), 5733–5752.

Marshall, J., D. Jamous, and J. Nilsson (1999), Reconciling thermodynamic and dynamic methods of computation of water-mass transformation rates, *Deep Sea Res., Part I*, *46*(4), 545–572.

Melling, H. (1993), The formation of a haline shelf front in wintertime in an ice-covered Arctic Sea, *Cont. Shelf Res.*, *13*(10), 1123–1147.

Melling, H., and E. Lewis (1982), Shelf drainage flows in the Beaufort Sea and their effect on the Arctic Ocean pycnocline, *Deep Sea Res., Part A*, *29*(8), 967–985.

Morison, J., R. Kwok, C. Peralta-Ferriz, M. Alkire, I. Rigor, R. Andersen, and M. Steele (2012), Changing Arctic Ocean freshwater pathways, *Nature*, *481*(7379), 66–70.

Nguyen, A. T., D. Menemenlis, and R. Kwok (2011), Arctic ice-ocean simulation with optimized model parameters: Approach and assessment, *J. Geophys. Res.*, *116*, C04025, doi:10.1029/2010JC006573.

Nurser, A. G., and J. C. Marshall (1991), On the relationship between subduction rates and diabatic forcing of the mixed layer, *J. Phys. Oceanogr.*, *21*, 1793–1802.

Onogi, K., et al. (2007), The JRA-25 reanalysis, *J. Meteorol. Soc. Jpn. Ser. II*, *85*(3), 369–432.

Proshutinsky, A., R. Krishfield, M.-L. Timmermans, J. Toole, E. Carmack, F. McLaughlin, W. J. Williams, S. Zimmermann, M. Itoh, and K. Shimada (2009), Beaufort Gyre freshwater reservoir: State and variability from observations, *J. Geophys. Res.*, *114*, C00A10, doi:10.1029/2008JC005104.

Spall, M. A., R. S. Pickart, P. S. Fratantoni, and A. J. Plueddemann (2008), Western Arctic shelfbreak eddies: Formation and transport, *J. Phys. Oceanogr.*, *38*(8), 1644–1668.

Steele, M., J. Morison, W. Ermold, I. Rigor, M. Ortmeyer, and K. Shimada (2004), Circulation of summer Pacific halocline water in the Arctic Ocean, *J. Geophys. Res.*, *109*, C02027, doi:10.1029/2003JC002009.

Stommel, H. M. (1979), Determination of water mass properties of water pumped down from the Ekman layer to the geostrophic flow below, *Proc. Nat. Acad. Sci.*, *76*, 3051–3055.

Timmermans, M.-L. (2015), The impact of stored solar heat on Arctic sea ice growth, *Geophys. Res. Lett.*, *42*, 6399–6406.

Timmermans, M.-L., and S. R. Jayne (2016), The Arctic Ocean spices up, *J. Phys. Oceanogr.*, *46*(4), 1277–1284.

Timmermans, M.-L., and A. Proshutinsky (2016), [The Arctic] Sea surface temperature [in "State of the Climate in 2015"], *Bull. Am. Meteorol. Soc.*, *97*(8), S137–S138.

Timmermans, M.-L., et al. (2014), Mechanisms of Pacific summer water variability in the Arctic's Central Canada Basin, *J. Geophys. Res.*, *119*, 7523–7548, doi:10.1002/2014JC010273.

Toole, J., R. Krishfield, M.-L. Timmermans, and A. Proshutinsky (2011), The Ice-Tethered Profiler: Argo of the Arctic, *Oceanography*, *24*(3), 126–135.

Weingartner, T. J., D. J. Cavalieri, K. Aagaard, and Y. Sasaki (1998), Circulation, dense water formation, and outflow on the northeast Chukchi Shelf, *J. Geophys. Res.*, *103*(C4), 7647–7661.

Wells, M., and J. Wettlaufer (2007), The long-term circulation driven by density currents in a two-layer stratified basin, *J. Fluid Mech.*, *572*, 37–58.

Williams, W. J., and E. C. Carmack (2015), The interior shelves of the Arctic Ocean: Physical oceanographic setting, climatology and effects of sea-ice retreat on cross-shelf exchange, *Prog. Oceanogr.*, *139*, 24–41.

Woodgate, R. A., K. Aagaard, J. H. Swift, K. K. Falkner, and W. M. Smethie (2005a), Pacific ventilation of the Arctic Ocean's lower halocline by upwelling and diapycnal mixing over the continental margin, *Geophys. Res. Lett.*, *32*, L18609, doi:10.1029/2005GL023999.

Woodgate, R. A., K. Aagaard, and T. J. Weingartner (2005b), A year in the physical oceanography of the Chukchi Sea: Moored measurements from autumn 1990–1991, *Deep Sea Res., Part II*, *52*(24), 3116–3149.

Woodgate, R. A., K. M. Stafford, and F. G. Prahl (2015), A synthesis of year-round interdisciplinary mooring measurements in the Bering Strait (1990–2014) and the RUSALCA years (2004–2011), *Oceanography*, *28*(3), 46–67.